Mon. Not. R. Astron. Soc. **000**, 1–?? (2002)   Printed 28 September 2010   (MN LaTeX style file v2.2)

arXiv:1009.5235v1 [astro-ph.CO] 27 Sep 2010

A survey of Low Luminosity Compact sources and its implication for evolution of radio-loud AGNs. I. Radio data

M. Kunert-Bajraszewska[1]*, M. P. Gawroński[1], A. Labiano[2] and A. Siemiginowska[3]
[1] *Toruń Centre for Astronomy, N. Copernicus University, Gagarina 11, 87-100 Toruń, Poland*
[2] *European Space Agency (ESA), European Space Astronomy Centre (ESAC), 28691 Villanueva de la Canada, Madrid, Spain*
[3] *Harvard-Smithsonian Centre for Astrophysics, 60 Garden St., Cambridge, MA 02138, USA*

Accepted 1988 December 15. Received 1988 December 14; in original form 1988 October 11

ABSTRACT

We present a new sample of Compact Steep Spectrum (CSS) sources with radio luminosity below 10^{26} W Hz^{-1} at 1.4 GHz called the low luminosity compact (LLC) objects. The sources have been selected from FIRST survey and observed with MERLIN at L-band and C-band. The main criterion used for selection was luminosity of the objects and approximately one third of the CSS sources from the new sample have a value of radio luminosity comparable to FR Is. About 80% of the sources have been resolved and about 30% of them have weak extended emission and disturbed structures when compared with the observations of higher luminosity CSS sources. We studied correlation between radio power and linear size, and redshift with a larger sample that included also published samples of compact objects and large scale FR IIs and FR Is. The low luminosity compact objects occupy the space in radio power versus linear size diagram below the main evolutionary path of radio objects. We suggest that many of them might be short-lived objects, and their radio emission may be disrupted several times before becoming FR IIs. We conclude that there exists a large population of short-lived low luminosity compact objects unexplored so far and part of them can be precursors of large scale FR Is.

Key words: galaxies: active – galaxies: evolution

1 INTRODUCTION

Radio sources are divided into two distinct morphological groups of objects: FR Is and FR IIs (Fanaroff &Riley 1974). There is a relatively sharp luminosity boundary between them at low frequency. The nature of the FR-division is still an open issue, as are the details of the evolutionary process in which younger and smaller Gigahertz-Peaked Spectrum (GPS) and Compact Steep Spectrum (CSS) sources become large scale radio structures. It is unclear whether FR II objects evolve to become FR Is, or whether a division has already occurred amongst CSS sources and some of these then become FR Is and some FR IIs. A majority of CSS sources known to date have high radio luminosities and, if unbeamed, have FR II structures. It seems reasonable to suspect that some of the CSSs with lower radio luminosity could be the progenitors of less luminous FR I objects.

The GPS and CSS sources form a well-defined class of compact radio objects and are considered to be entirely contained within the host galaxy. During their evolution the radio jets start to cross the ISM and try to leave the host galaxy. The interaction with the ISM can be very strong in GPS/CSS sources (Holt et al. 2006; Labiano et al. 2005) and it seems to be a crucial point in the evolution of radio sources. Recently developed models (Kaiser & Best 2007) show that all sources start out with a FR II morphology. As the radio source expands the interaction with the dense environment of the host galaxy can disrupt jets and change their morphology to FR Is or hybrid objects (Gopal-Krishna & Wiita 2000; Gawroński et al. 2006). Some sources with disrupted jets can fade away (Alexander 2000). Detection of several candidates for dying compact sources supports this view (Giroletti et al. 2005; Kunert-Bajraszewska et al. 2005, 2006; Marecki et al. 2006). What's more, the activity of compact radio sources can be an episodic event (Snellen et al. 1999; Marecki et al. 2003b; Gugliucci et al. 2005; Kunert-Bajraszewska et al. 2006), like in the case of large scale radio objects.

As recently suggested by Czerny et al. (2009) there could be a connection between the existence of short-lived compact radio sources and the intermittent activity of the central engine caused by a radiation pressure instability within an accretion disc. According to the authors a radio source powered by a short-lived outburst of the central ac-

---

* E-mail: magda@astro.uni.torun.pl

tivity is not able to escape from the host galaxy unless the active phase lasts longer than ∼10^4 years. It is then likely that among the low luminosity compact (LLC) sources we can find objects affected during their evolution either by a strong interaction with the ISM, which changes their morphology and luminosity, or by the instability of the accretion disc.

In this paper we present the L-band and C-band MERLIN observations of 44 low luminosity CSS sources selected from the FIRST survey. This is a new approach since the main criterion used for selection was not flux density but luminosity of the objects. The selection criteria caused that approximately one third of the CSS sources from the new sample have a value of radio luminosity lower than the luminosity boundary found for FR sources (Fanaroff &Riley 1974), which means that they are compact young sources with luminosities comparable to FR Is (Fig. 4). The goal of this project is to study the properties of low luminosity compact (LLC) objects and the evolution of the compact object population. Our previous multifrequency observations of CSS sources have shown that some of the small-scale objects can be strong candidates for compact faders (Kunert-Bajraszewska et al. 2005, 2006). This finding supports the idea that there exist a group of short-lived radio objects that has been largely neglected to date.

2 SELECTION AND OBSERVATIONS OF A NEW SAMPLE

Using the final release of FIRST, combined with the GB6 survey at 4.85 GHz we looked for unresolved, isolated sources i.e. more compact than FIRST beam ($5''\!.4$) and surrounded by an empty field (we adopted $1'$ as a radius of that field). We required that the redshifts of the objects identified with radio sources are known and we extracted them from NED and Sloan Digital Sky Survey (SDSS). Consequently, we were able to impose the low power criterion. The limit on flux density was chosen in order to produce a sample of manageable size, but also to exclude objects with flux densities too low to be detected in snapshot observations. Eventually, the selection criteria were as follows:

- Low luminosity criterion: $L_{1.4\rm GHz} < 10^{26}$ W Hz^{-1}. (for H$_0$=100 km s^{-1} Mpc^{-1}, q_0=0.5; in this paper we use another cosmology);
- Flux density criterion: 70 mJy $\leqslant S_{1.4\rm GHz} \leqslant$ 1 Jy;
- Spectral index criterion: $\alpha_{1.4\rm GHz}^{4.85\rm GHz} > 0.7$ ($S \propto \nu^{-\alpha}$).

Finally, the new sample consists of 44 sources (Table 2).

The initial survey was undertaken using MERLIN at L-band. Then some of the sources were also observed with MERLIN at C-band. All the L-band snapshot observations were made between December 2006 and May 2007. Additional C-band snapshot observations were made in 2008 and 2009. Each target source together with its associated phase reference sources was observed for ∼60 min including telescope drive times. The preliminary data reduction was made using an AIPS-based PIPELINE procedure developed at JBO. The resulting phase-calibrated images created with PIPELINE were further improved using several cycles of self-calibration and imaging, the final total intensity (I) and polarization intensity (P) images being produced using the task IMAGR. We considered only emission above 3σ noise level, and we blanked out all the points for which observed $P < 3\sigma$, to avoid possible mis-use of low signal-to-noise polarization data. The flux densities of the main components of the target sources were then measured, by fitting Guassian models to the components in the image, using task JMFIT (Table 2). For more extended features the flux densities were evaluated by means of IMSTAT. Sub–components are referred to as North (N), South (S), East (E), West (W) and Central (C). When a component is split into more pieces, a digit (1,2, etc.) is added (e.g. N1, N2). The position of the optical counterparts of target sources are marked with a cross in the images and are taken from the SDSS (found within the radius of $10''$ from the radio source) or from the literature. The feature in the radio image closest to the cross is indicated as 'C' and treated as probable radio core.

Based upon available radio images (our MERLIN L-band and C-band observations and other found in the literature), the new sources have been divided into four categories (Table 2). However, for most of the sources described here we have observation only at one frequency and their classification should be treated as the preliminary one ('?' means the most uncertain classification). 'Single' means the source is a pointlike object unresolved or slightly resolved. 'Core-jet' is a source with a bright central component and a one- or two-sided emission (jets). 'Double-lobed' objects show at least two kinds of morphologies. Some of them consist of two point-like components without a visible radio core in available radio images, whereas the others show a central weak component and distorted extended structure on both sides of it. Many of the double objects also show brightness asymmetry. For some of them (those with probable core detection) we were able to evaluate the flux density ratio, r_s, defined to be >1, of the oppositely directed components. The last category, 'other', comprises sources with peculiar morphologies: three objects have distorted radio morphologies, other three have only a single visible lobe, and one object is resolved into four components with high-resolution imaging. Fig. 1, Fig. 2 and Fig. 3 show images of the sources with resolved structures with the exception of one object (1641+320) which will be described in a separate paper.

In this paper, we present the analysis of MERLIN radio observations of a new sample of low luminosity CSS sources and the study the correlation between radio power and linear size, and redshift, making use of a larger sample that included also published samples of CSS sources by Fanti et al. (2001) and Marecki et al. (2003a). The combined sample of CSS sources we used in our study is gathered in Table A1 (see Appendix). The optical data of the sample of low luminosity CSS sources will be discussed in a forthcoming paper (Kunert-Bajraszewska & Labiano,2010; hereafter Paper II).

Throughout the paper, we assume a cosmology with H$_0$=71 km s^{-1} Mpc^{-1}, Ω_M=0.27, Ω_Λ=0.73.

3 NOTES ON INDIVIDUAL SOURCES

0025+006. The 1.6 GHz MERLIN map (Fig. 1) shows an asymmetric morphology: the brightest central component is probably a radio core and the extended south-eastern emission is a radio jet (E).

0801+437. This source is unresolved in 1.6 GHz MER-

Table 1. Basic parameters of 44 target sources

Source Name (1)	RA h m s (2)	Dec ° ′ ″ (3)	ID (4)	z (5)	$S_{1.4}$ Jy (6)	$\log L_{1.4}$ W Hz^{-1} (7)	$S_{4.85}$ Jy (8)	$\log L_{4.85}$ W Hz^{-1} (9)	$\alpha^{4.85}_{1.4}$ (10)	LLS h^{-1} kpc (11)	Type (12)
0025+006	00:28:33.42	00:55:11.00	G	0.104	0.219	24.77	0.081	24.34	0.80	3.13	Cj?
0754+401	07:57:56.69	39:59:36.00	G	0.066	0.098	24.00	0.030	23.49	0.95	0.25	S
0801+437	08:04:54.91	43:35:37.20	G	0.123*	0.352	25.13	0.135	24.72	0.77	0.44	D?
0810+077	08:13:23.76	07:34:05.80	Q	0.112	0.435	25.14	0.158	24.70	0.82	2.78	D?
0821+321	08:25:04.55	31:59:57.30	G	0.265	0.076	25.21	0.030	24.81	0.75	7.69	D
0835+373	08:38:25.00	37:10:36.90	Q	0.396	0.383	26.32	0.148	25.91	0.76	1.01	S
0846+017	08:48:56.56	01:36:47.40	G	0.349	0.085	25.54	0.034	25.14	0.74	6.12	Cj
0850+024	08:53:14.23	02:14:53.70	G	0.460	0.112	25.94	0.034	25.42	0.96	5.98	D
0851+024	08:54:08.45	02:13:15.80	G	0.399	0.118	25.82	0.039	25.33	0.89	3.41	D
0854+210	08:57:20.98	20:48:53.80	G	0.032	0.082	23.27	0.033	22.87	0.76	1.76	O
0907+049	09:09:51.13	04:44:22.13	G	0.640p	0.178	26.49	0.049	25.93	1.04	8.32	D?
0914+114	09:17:16.38	11:13:36.90	G	0.178*	0.742	25.81	0.124	25.03	1.44	0.68	O
0914+504	09:17:34.82	50:16:38.20	Q	0.633	0.104	26.24	0.039	25.82	0.79	4.86	D
0921+143	09:24:05.29	14:10:21.60	Q	0.135	0.105	24.69	0.031	24.17	0.98	0.73	Cj
0923+079	09:26:07.99	07:45:26.60	Q	0.442	0.158	26.05	0.056	25.60	0.83	7.94	O
0931+033	09:34:30.74	03:05:45.50	G	0.225	0.280	25.61	0.119	25.24	0.69	1.61	Cj
0942+355	09:45:25.89	35:21:03.50	G	0.208	0.140	25.24	0.042	24.71	0.97	4.41	D
1007+142	10:09:55.51	14:01:54.30	Q	0.213	0.995	26.11	0.390	25.70	0.75	3.26	D
1009+053	10:12:04.73	05:06:13.20	G	0.460p	0.206	26.21	0.055	25.63	1.06	8.71	D?
1037+302	10:40:29.96	29:57:58.00	G	0.091	0.364	24.87	0.107	24.33	0.98	3.63	D
1053+505	10:56:28.21	50:19:52.20	Q	0.820	0.079	26.40	0.032	26.01	0.73	8.19	D
1140+058	11:43:11.03	05:35:15.90	Q	0.497	0.194	26.26	0.061	25.76	0.93	16.97	Cj
1154+435	11:57:27.60	43:18:06.80	Q	0.230	0.247	25.58	0.106	25.21	0.68	4.55	Cj
1156+470	11:59:19.99	46:45:44.80	G	0.467	0.081	25.82	0.031	25.40	0.77	4.98	O
1308+451	13:10:57.00	44:51:46.60	G	0.391	0.097	25.71	0.034	25.25	0.84	3.85	D?
1321+045	13:24:19.70	04:19:07.20	G	0.263	0.128	25.43	0.046	24.98	0.82	16.90	D
1359+525	14:00:51.62	52:16:06.60	G	0.118	0.170	24.78	0.064	24.35	0.78	0.42	S
1402+415	14:04:16.37	41:17:48.80	G	0.361	0.210	25.96	0.073	25.50	0.85	1.00	S
1407+363	14:09:42.46	36:04:16.00	G	0.148	0.141	24.91	0.045	24.41	0.92	0.07	Cj?
1411+553	14:13:27.21	55:05:29.30	G	0.282	0.126	25.49	0.033	24.91	1.08	0.80	S
1418+053	14:21:04.25	05:08:44.90	G	0.455	0.283	26.33	0.108	25.91	0.77	1.67	S
1506+345	15:08:05.68	34:23:23.30	Gp	0.045	0.121	23.75	0.044	23.31	0.81	0.15	O
1521+324	15:23:49.35	32:13:50.10	G	0.110	0.168	24.71	0.051	24.19	0.96	0.40	S
1532+303	15:34:09.90	30:12:04.00	q	0.001?	0.071	20.17	0.030	19.80	0.70	0.004	S
1542+390	15:43:49.49	38:56:01.40	G	0.553	0.189	26.36	0.049	25.77	1.09	8.08	D
1543+465	15:45:25.46	46:22:44.70	G	0.400	0.459	26.41	0.110	25.79	1.15	6.57	D?
1550+444	15:52:35.37	44:19:06.10	G	0.452	0.139	26.02	0.049	25.56	0.84	6.90	O
1558+536	15:59:27.66	53:30:54.70	G	0.179	0.170	25.17	0.058	24.71	0.86	5.08	D?
1601+528	16:02:46.39	52:43:58.70	G	0.106	0.557	25.19	0.208	24.76	0.79	0.38	D
1610+407	16:11:48.55	40:40:20.90	G	0.151	0.553	25.52	0.166	25.00	0.97	2.60	Cj?
1624+049	16:26:50.30	04:48:50.50	G	0.040p	0.162	23.77	0.056	23.31	0.85	1.94	D
1641+320	16:43:11.35	31:56:18.00	Qb	0.586	0.113	26.20	0.041	25.76	0.82	10.56	O†
1715+499	17:16:46.34	49:56:44.30	G	0.628	0.095	26.20	0.035	25.76	0.80	2.38	D
1717+547	17:18:54.40	54:41:48.20	G	0.147	0.323	25.26	0.110	24.80	0.87	0.18	D

Description of the columns: (1) source name; (2) and (3) source coordinates (J2000) extracted from FIRST; (4) optical identification: G - galaxy, Q - quasar, q - star-like object, Gp - galaxy pair, Qb - binary quasar; (5) redshift; 'p' means photometric redshift taken from literature or SDSS; '?' means the spectroscopic redshift is very uncertain because of a poor quality of the spectrum; ∗ means uncertain redshift probably belongs to a random foreground galaxy; (6) total flux density at 1.4 GHz extracted from FIRST; (7) log of the radio luminosity at 1.4 GHz; (8) total flux density at 4.85 GHz extracted from GB6; (9) log of the radio luminosity at 4.85 GHz; (10) spectral index between 1.4 and 4.85 GHz calculated using flux densities in columns (6) and (8); (11) largest linear size (LLS) calculated based on the largest angular size measurements in the 1.4 GHz MERLIN image – in most cases, as a separation between the outermost component peaks, otherwise measured in the image contour plot; in the case of single sources the linear size means the upper limit estimated using deconvolved component major axis angular size from L-band MERLIN image; (12) radio morphology based on the available radio images, this is a simple classification in agreement with the Kunert-Bajraszewska & Thomasson (2009), more detailed description is in section 2; S - single means unresolved or slightly resolved in available radio image, Cj - core-jet, D - double-lobed, O - other, more complex structures; '?' means the most uncertain classification.

† 1641+320 will be described in a separate paper.

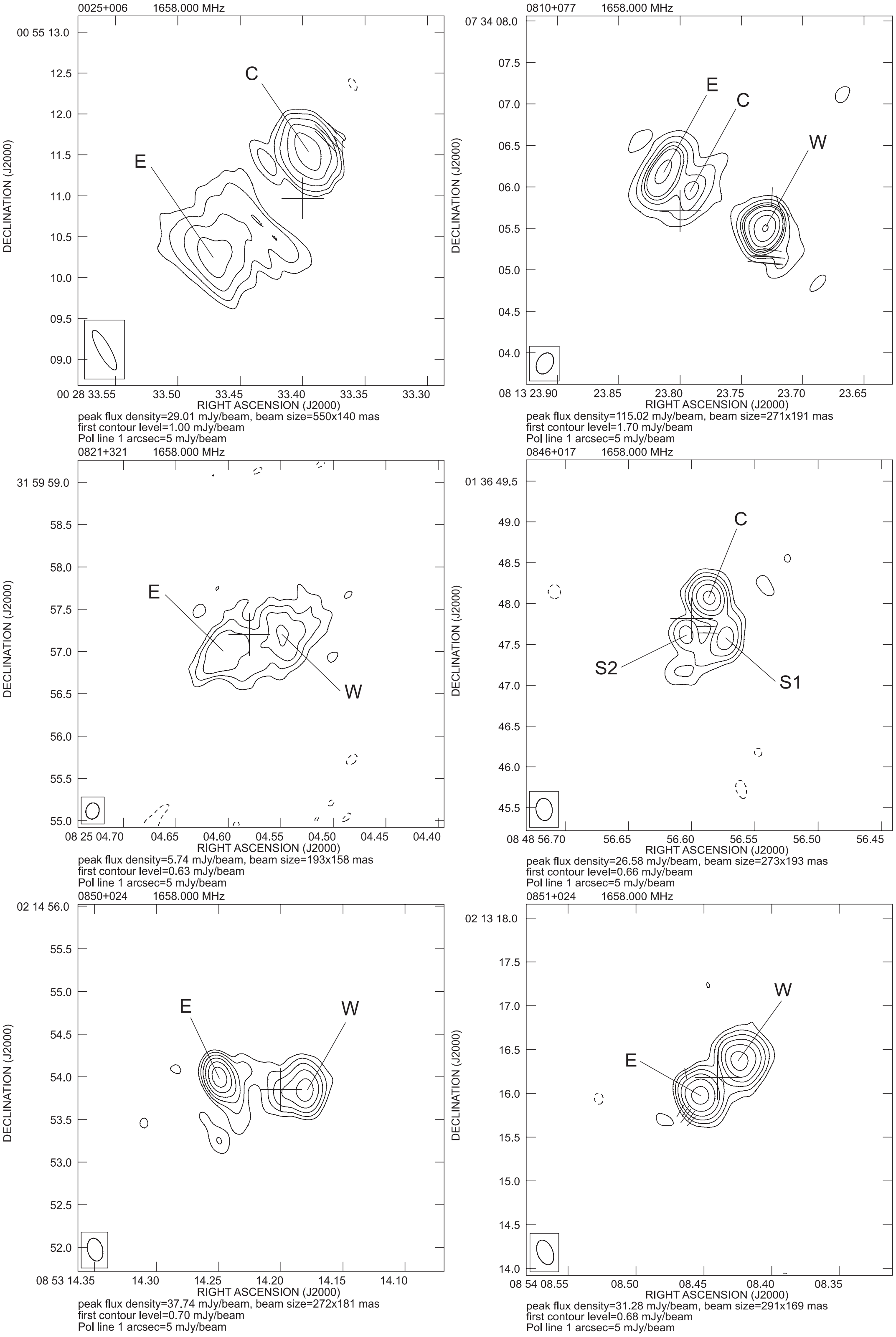

Figure 1. MERLIN L-band images. Contours increase by a factor 2, and the first contour level corresponds to $\approx 3\sigma$, vectors represent the polarized flux density. A cross indicates the position of an optical object found using the most actual version of SDSS/DR7.

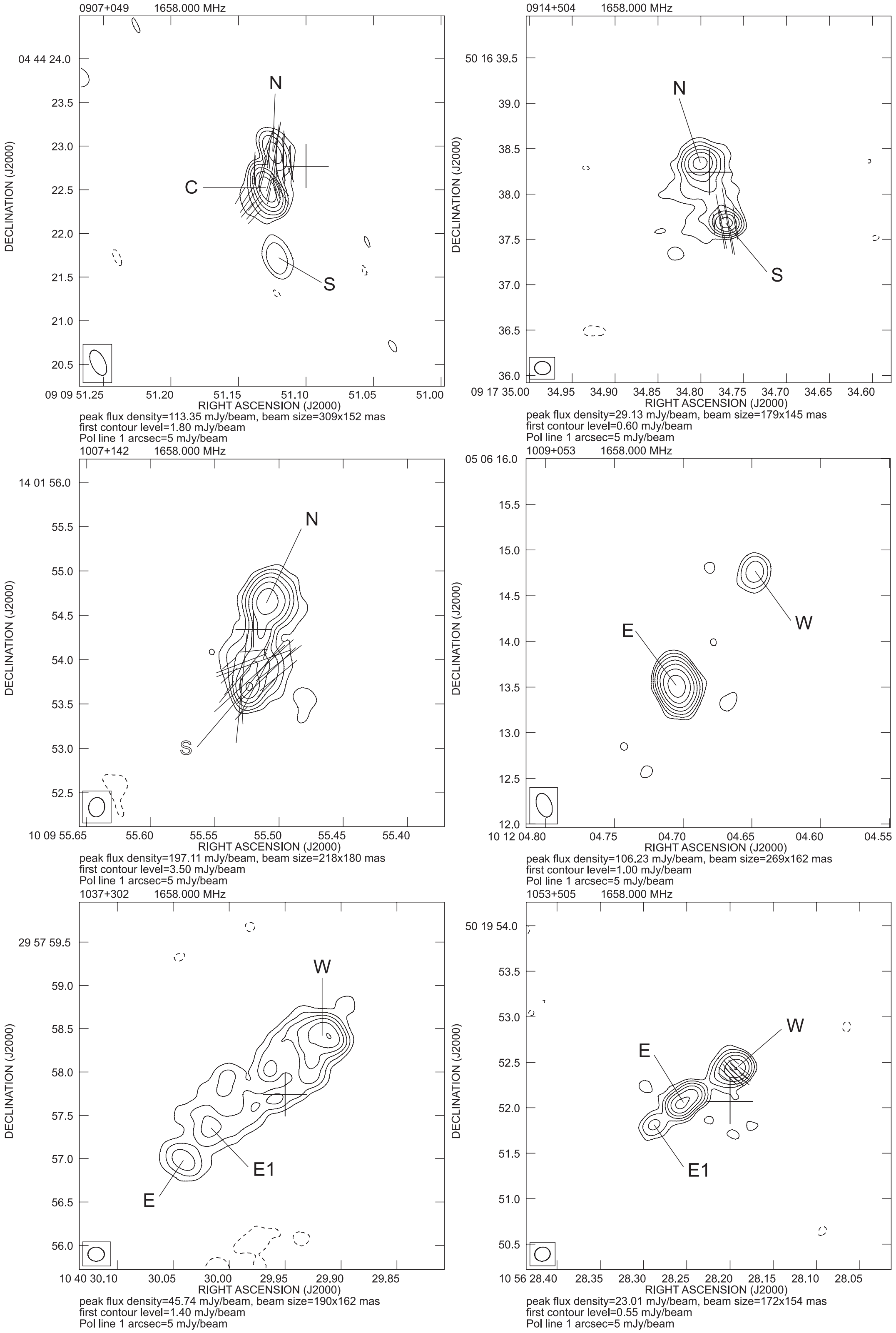

Figure 1. MERLIN L-band (cont.)

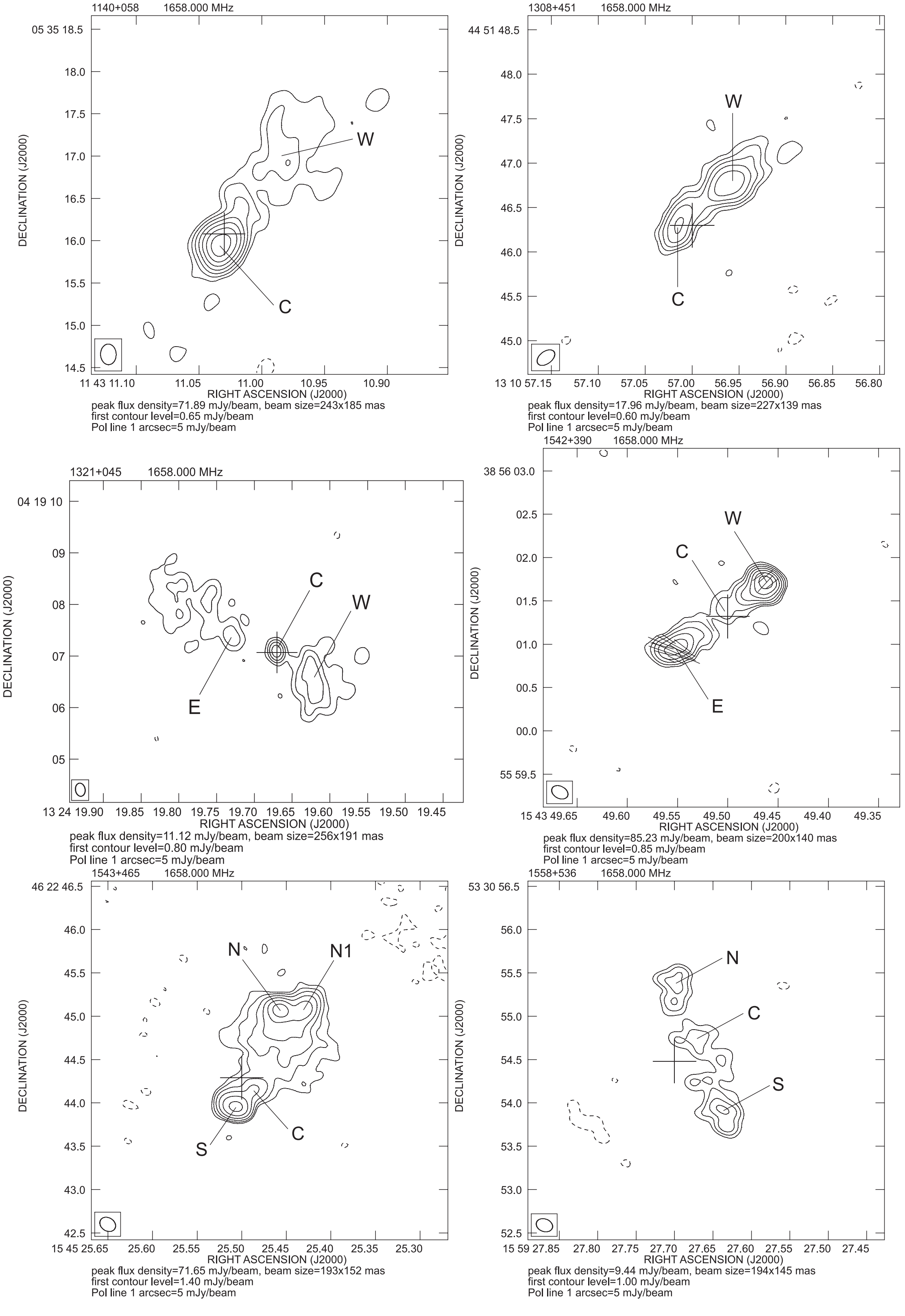

Figure 1. MERLIN L-band (cont.)

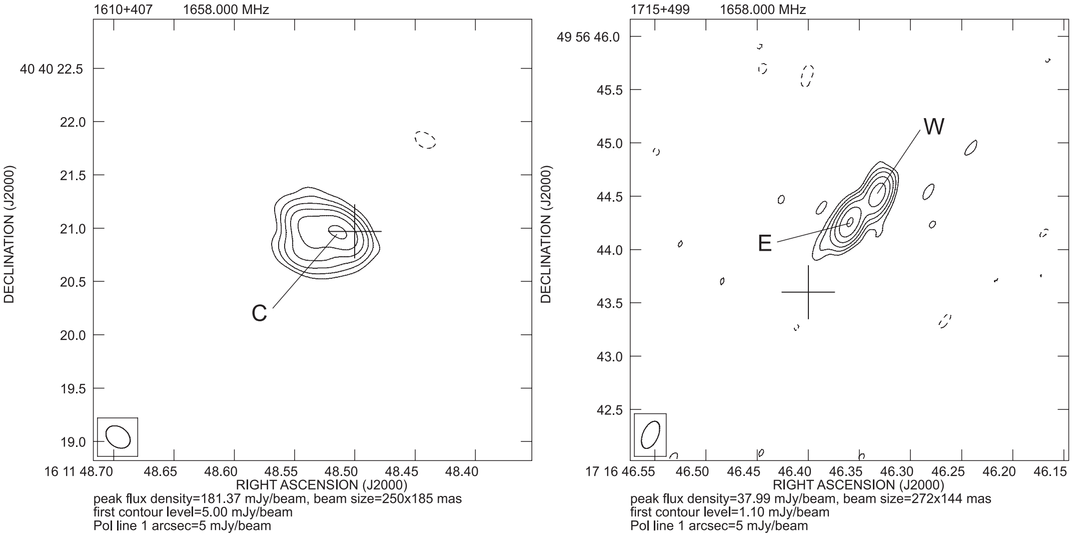

Figure 1. MERLIN L-band (cont.)

LIN observations and only 1.6 GHz EVN observations show structure classified as possible double by de Vries et al. (2009).

0810+077. This source has been classified as a possible double object (Fig. 1). The weak component (C) whose position is correlated with the position of the optical counterpart could be a radio core, on opposite sides of which there is emission from the two radio jets/lobes. The flux density ratio, r_s of the oppositely directed components E and W amounts to 1.7.

0821+321. This is a double object with two weak radio lobes without evidence of bright hotspots and radio core (Fig. 1).

0846+017. This is probably a core-jet morphology (Fig. 1) with the brightest component to be a radio core (C) and a bent radio jet (S1, S2).

0850+024. Compact double object (Fig. 1). The position of the optical counterpart probably indicates the position of the slightly resolved radio core.

0851+024. Compact double object with a symmetric morphology (Fig. 1).

0854+210. Weak radio galaxy with diffuse morphology (Fig. 2) also detected in infrared (Drake et al. 2003). The peak of emission in 1.6 GHz MERLIN image is a radio core also visible in 5 GHz MERLIN image (C).

0907+049. This is a double object with the brightest central component (C) probably containing a radio core, on opposite sides of which there is emission from the two radio jets/lobes (Fig. 1).However the polarization is not detected in the southern component, which can be an artifact. The polarized flux density of components C and N amounts to 3 mJy and 6 mJy, respectively.

0914+114. Both 1.6 GHz and 5 GHz MERLIN images show single component. This source has been resolved with VLBI at 2.3 GHz into complex structure consisting of four well separated components (Xiang et al. 2005).

0914+504. Quasar with a double morphology and asymmetric polarization. The luminosity of the polarized southern component is lower than the northern one, which can contain a radio core (Fig. 1). The polarized flux density of component S amounts to 4 mJy.

0921+143. The 1.6 GHz MERLIN observation shows a single component which is resolved in 5 GHz MERLIN image into probably core-jet morphology (Fig. 2).

0923+079. The 1.6 GHz morphology and the position of the optical counterpart suggest there is only a single lobe visible in this source (Fig. 3). This interpretation is in agreement with 5 GHz MERLIN image. The weak point emission is probably a radio core and the lobe indicated as 'N' in 1.6 GHz image breaks into weak and probably fading components in 5 GHz MERLIN image.

0931+033. The 1.6 GHz MERLIN observation shows a single component which is resolved in 5 GHz MERLIN image into probably core-jet morphology (Fig. 2).

0942+355. This is a double object with asymmetric emission from two radio lobes (Fig. 2). The position of the optical counterpart is correlated with a weak central emission (C). The 5 GHz MERLIN image shows only an emission from the south-eastern radio lobe (E) with a steep spectrum $\alpha_{1.6}^{5.0} = 1.1$. The flux density ratio, r_s of the oppositely directed components E and W amounts to 2.3.

1007+142. Radio galaxy with a double morphology (Fig. 1). Large variations of polarization angle are seen in the southern lobe. The luminosity of the polarized southern component is lower than the northern one. The polarized flux density of component S amounts to 8.5 mJy.

1009+053. Two components with different brightness are visible (Fig. 1). Since the position of the optical counterpart is outside the image range it is difficult to interpret the structure.

1037+302. The 1.6 GHz MERLIN image shows a highly asymmetric double object (Fig. 1) also detected with the VLA at 8.4 GHz and 22.5 GHz by Giroletti et al. (2005). The position of the optical counterpart is well correlated with radio core observed in 1.6 GHz VLBA image (Giroletti et al. 2005). Our 5 GHz MERLIN image shows only an emission from the north-western radio lobe (W) and is not published here. Although the brightness asymmetry is visible in this source, the diffused extended emission is difficult to mea-

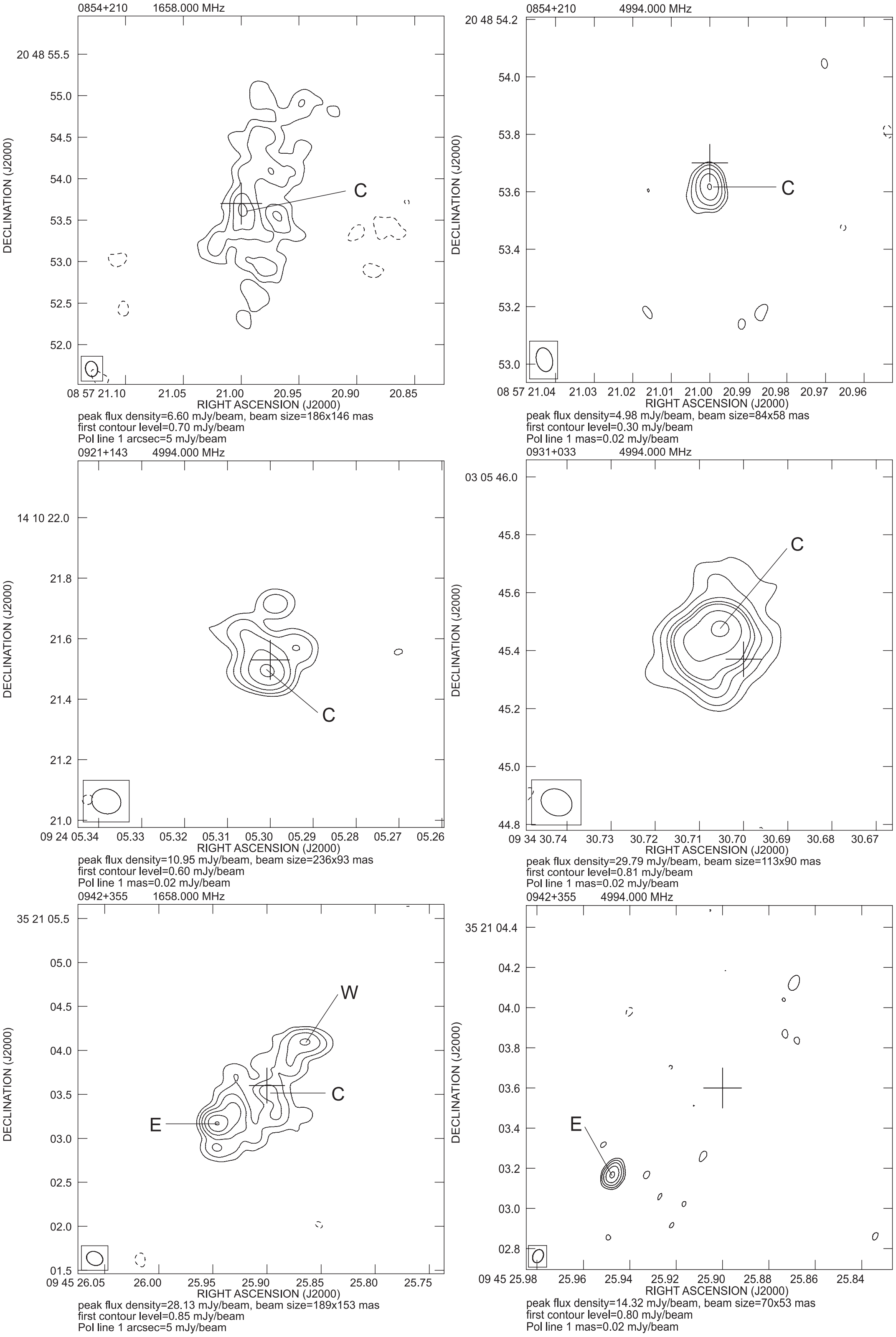

Figure 2. MERLIN L-band and C-band images. Contours increase by a factor 2, and the first contour level corresponds to $\approx 3\sigma$, vectors represent the polarized flux density. A cross indicates the position of an optical object found using the most actual version of SDSS/DR7.

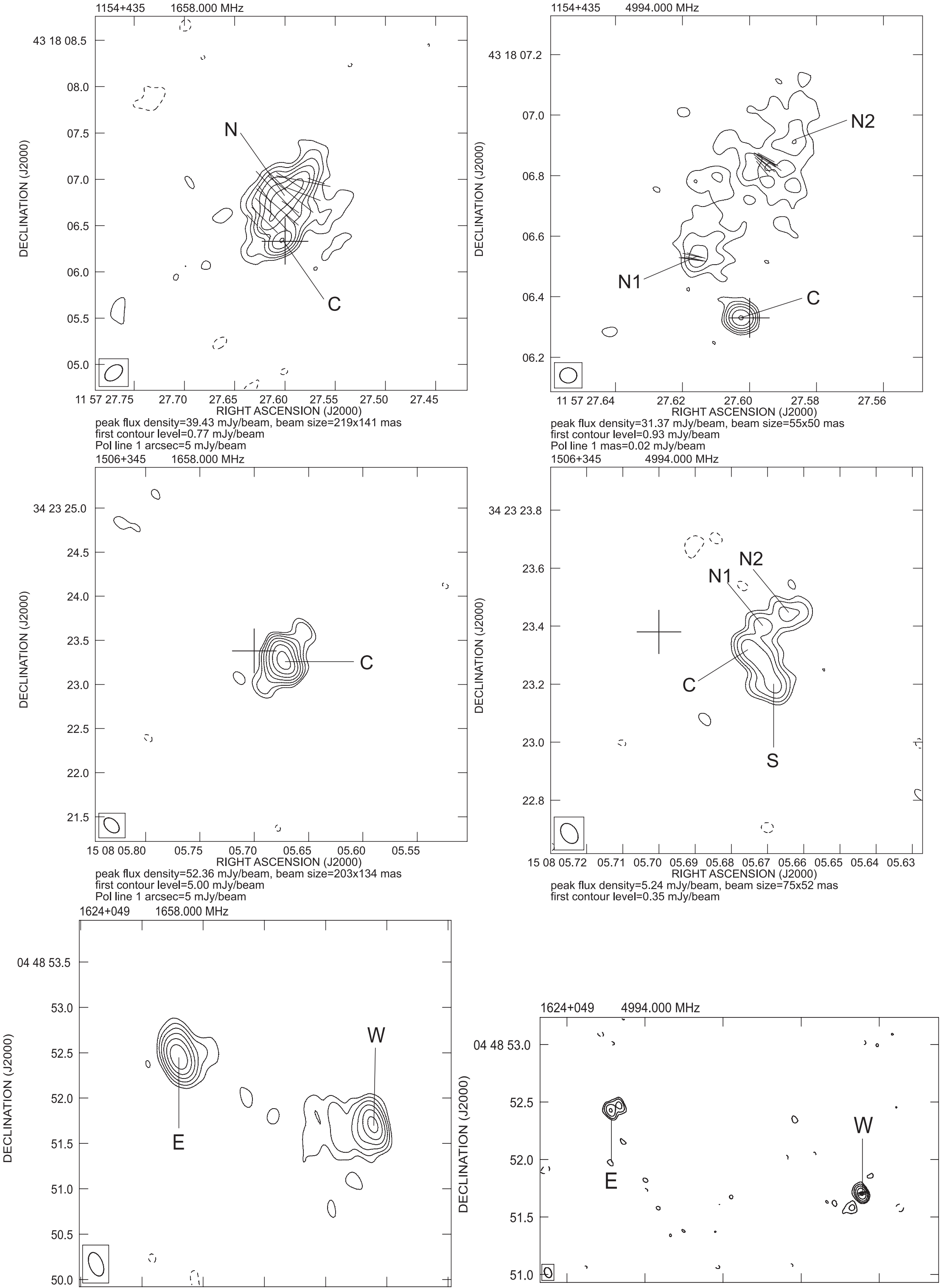

Figure 2. MERLIN L-band and C-band images (cont.)

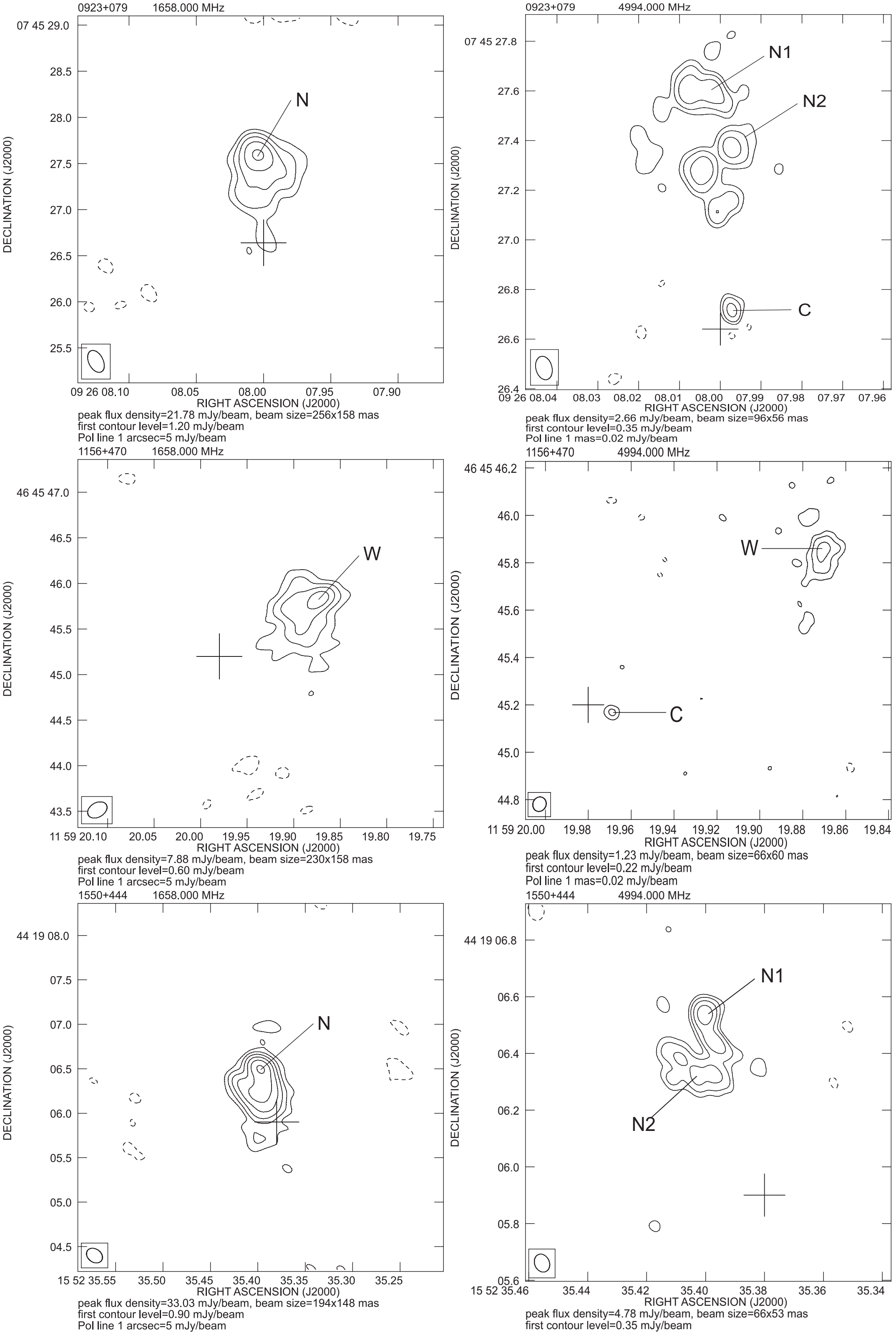

Figure 3. MERLIN L-band and C-band images of 'single-lobed' objects. Contours increase by a factor 2, and the first contour level corresponds to $\approx 3\sigma$, vectors represent the polarized flux density. A cross indicates the position of an optical object found using the most actual version of SDSS/DR7.

Table 2. Flux densities of sources principal components from the 1.6 GHz and 5 GHz MERLIN images

Source name (1)	Components (2)	$S_{1.6\,\mathrm{GHz}}$ mJy (3)	$S_{5\,\mathrm{GHz}}$ mJy (4)	Source name (1)	Components (2)	$S_{1.6\,\mathrm{GHz}}$ mJy (3)	$S_{5\,\mathrm{GHz}}$ mJy (4)
0025+006	C	66	–	1140+058	C	125	–
	E	41	–		W	22	–
0810+077	C	53	–	1154+435	C	36	32
	E	103	–		N	186	–
	W	175	–		N1	–	17
0821+321	E	35	–		N2	–	9
	W	33	–	1156+470	C	–	0.5
0846+017	C	36	–		W	30	4
	S1	15	–	1308+451	C	32	–
	S2	6	–		W	59	–
0850+024	E	44	–	1321+045	C	13	–
	W	38	–		E	38	–
0851+024	E	50	–		W	49	–
	W	53	–	1506+345	C	99†	14
0854+210	C*	57	6		N1	–	4
0907+049	C	123	–		N2	–	3
	N	21	–		S	–	8
	S	8	–	1542+390	C	4	–
0914+504	N	51	–		E	53	–
	S	32	–		W	119	–
0921+143	C	–	18	1543+465	C	9	–
0923+079	N	62	–		N	127	–
	C	–	1.5		N1	90	–
	N1	–	8		S	99	–
	N2*	–	7	1550+444	N	98	–
0931+033	C	–	83		N1	–	11
0942+355	C	11	–		N2*	–	7
	E	61	18	1558+536	C	6	–
	W	26	–		N	21	–
1007+142	N	482	–		S	28	–
	S	291	–	1610+407	C	514	–
1009+053	E	150	–	1624+049	E	69	13
	W	9	–		W	47	15
1037+302	E	26	–	1715+499	E	46	–
	E1	16	–		W	33	–
	W	171	–				
1053+505	E	40	–				
	E1	6	–				
	W	32	–				

∗ - sum of the visible components, † - the whole source

sure and consequently the flux density ratio is difficult to evaluate.

1053+505. Three components are visible in 1.6 GHz MERLIN image (Fig. 1). The polarization is detected only in the north-western component (W), whose luminosity is lower than the eastern one (E). The polarized flux density of component W amounts to 3 mJy. It is difficult to classify this source without a 5 GHz image. This is probably a double object with emission from two radio lobes/jets.

1140+058. This is a core-jet quasar (Fig. 1).

1154+435. The 1.6 GHz MERLIN image of this source shows a complicated (double?) morphology. The magnetic field appears to be ordered and follows the direction of the jet visible at higher frequency. The polarized flux density of component N amounts to 4 mJy. The 5 GHz MERLIN image shows one bright component, a radio core (C) with a flat spectrum $\alpha^{5.0}_{1.6} = 0.1$, and diffuse northern emission which could be a bent radio jet (Fig. 2). The polarization is visible in two places, where we have peaks of emission and where the jet interacts with the surrounding medium.

1156+470. The 1.6 GHz morphology and the position of the optical counterpart suggest there is only a single lobe visible in this source (Fig. 3). The 5 GHz MERLIN image shows very weak component 'C' which is probably a radio core and fading lobe 'W'.

1308+451. This could be a double or a core-jet object (Fig. 1).

1321+045. The position of the central bright component visible in 1.6 GHz MERLIN image (Fig. 1) is well correlated with the position of the optical counterpart suggesting it is a radio core (C), on opposite sides of which there is diffuse emission from the two radio jets/lobes. The flux density ratio, r_s of the oppositely directed components E and W amounts to 1.3.

1407+363. This source is unresolved in 1.6 GHz MERLIN observations. It is classified as a core-jet based on the 1.6 GHz EVN+VLBA image (de Vries et al. 2009).

1506+345. A point-like object visible in 1.6 GHz MERLIN image (Fig. 2) is resolved into complicated structure in 5 GHz MERLIN image. High resolution 1.6 GHz EVN observations of this sources (de Vries et al. 2009) show two components: the compact one (indicated as 'C' in our image) and very weak extended component (probably 'S' in our 5 GHz MERLIN image). According to the optical observations (Mazzarella et al. 1993) it is an interacting galaxy pair separated by $24''$. The radio emission is probably associated with the north-eastern member of this galaxy pair and its disturbed structure is probably a consequence of the galaxy-galaxy interactions.

1542+390. This is a double object (Fig. 1) with a weak central emission which could be a radio core (C). There is an asymmetry in polarization between components E and W, and their polarized flux density amounts to 4 mJy and 1.5 mJy, respectively. The flux density ratio, r_s of the oppositely directed components E and W amounts to 2.2.

1543+465. A double galaxy with an asymmetric structure (Fig. 1). A weak component indicated as C could be a radio core. Assuming that C is indeed a radio core the flux density ratio, r_s of the oppositely directed components N+N1 and S amounts to 2.2. However, without an observation at higher frequency the identification of the components is uncertain.

1550+444. The 1.6 GHz morphology and the position of the optical counterpart suggest there is only a single lobe visible in this source (Fig. 3). The 5 GHz MERLIN image shows weak structure with a peak of emission indicated as 'N1'.

1558+536. This is a galaxy with a double-like radio morphology. Probably one of the weak central components can contain a radio core (Fig. 1). Assuming that C is indeed a radio core the flux density ratio, r_s of the oppositely directed components N and S amounts to 1.3.

1601+528. This source is unresolved in 1.6 GHz MERLIN observations. It is classified as double based on the 1.6 GHz and 5 GHz EVN and VLBA observations (de Vries et al. 2009).

1610+407. This is probably a core-jet object (Fig. 1), but this classification is uncertain since this structure show more details at higher frequency (de Vries et al. 2009).

1624+049. This is a galaxy with a double radio morphology visible in both 1.6 GHz and 5 GHz MERLIN observations (Fig. 2). Both components have steep spectrum: $\alpha_{1.6}^{5.0} = 1.5$ (E) and $\alpha_{1.6}^{5.0} = 1.0$ (W) and they are probably radio lobes. The flux density ratio, r_s of the components E and W amounts to 1.5 and 1.15 at 1.6 and 5 GHz, respectively.

1715+499. This is a compact double object (Fig. 1).

1717+547. This source is unresolved in 1.6 GHz MERLIN observations. It is classified as double based on the 1.6 GHz and 5 GHz EVN and VLBA observations (de Vries et al. 2009).

4 DISCUSSION

The new sample of Low Luminosity Compact (LLC) sources that we present in this paper consists of 44 objects. We calculated their basic physical parameters and gathered them in Table 2. In Fig. 4 we compare their luminosity and linear radio size with the sources from other samples. We used combined sample of CSS sources (Table A1, Appendix), GPS/high-frequency peaked (HFP) sources from master list created by Labiano et al. (2007) and the revised 3C sample of FR I and FR II sources (LRL sample, Laing at al. (1983)) for comparison and statistical study. The Luminosity-Size diagram (Fig. 4a) shows an evolutionary scheme of radio-loud AGNs. The selection criteria used for the new sample resulted in approximately one third of the LLC sources having a value of the 1.4 GHz radio luminosity comparable to FR Is. Their luminosities are definitely lower than CSS sources from last existing samples (crosses in Fig. 4a). About 70% of the sources from the sample are galaxies and all of them are nearby objects with redshifts in the range $0.04 < z < 0.9$, although the value of the redshift was not a selection criterion (Fig. 4b).

4.1 Characteristic of the groups of objects

About 80% of the sources in our sample are resolved in available radio maps (this paper and the literature), and at least (Table 2) 39% of the resolved objects are classified as double-lobed, although in this category we do put compact doubles without visible core and those with weak central component detected. A large precentage (∼86%) of these objects show asymmetry in components brightness, but we have measured the flux density ratio only for those with probable core detection (see Section 3). The observed asymmetry among LLC sources is consistent with the previous finding for the CSS source population (Saikia et al. 2001) namely that, as a class, the CSSs are more asymmetric than larger radio sources of similar power. For one source, 0942+355, the brightness asymmetry of the components (probably radio lobes) is also visible in 5 GHz image (Fig. 2). The 1037+302 has already been observed and investigated at higher frequencies with the VLA (Giroletti et al. 2005). The very weak peak of emission visible in our 1.6 GHz MERLIN image (Fig. 1), well correlated with the position of the optical counterpart, appeared to be a very weak radio core at 22 GHz with VLA. According to Giroletti et al. (2005) this source will evolve to FR I. Two of the sources classified as double (0821+321, 1558+536) have breaking up structures without obvious signs of activity (Fig. 1). About 70 % of the total flux density is missing in the MERLIN L-band image of weak 1558+536, suggesting that the diffuse emission is resolved in our observations.

We have detected polarization for some of the double sources (Fig. 1). These are doubles without a visible radio core or a very weak one (0914+504, 1007+142, 1053+505, 1542+390). The flux density and luminosity of the polarized component are lower than those of the second component (Table 2). Again there is visible asymmetry here, which can be explained in the terms of interaction of the source with an asymmetric medium in the central regions of the host elliptical galaxy. On the contrary to large radio objects, in GPS/CSS sources, the jet is still crossing the ISM and the interaction with the environment can be very strong. Observations of the ionized gas in GPS and CSS sources show the presence of such interactions (Holt et al. 2006; Labiano et al. 2005). The interactions with the ISM can be confirmed also by complicated structure of 1543+465

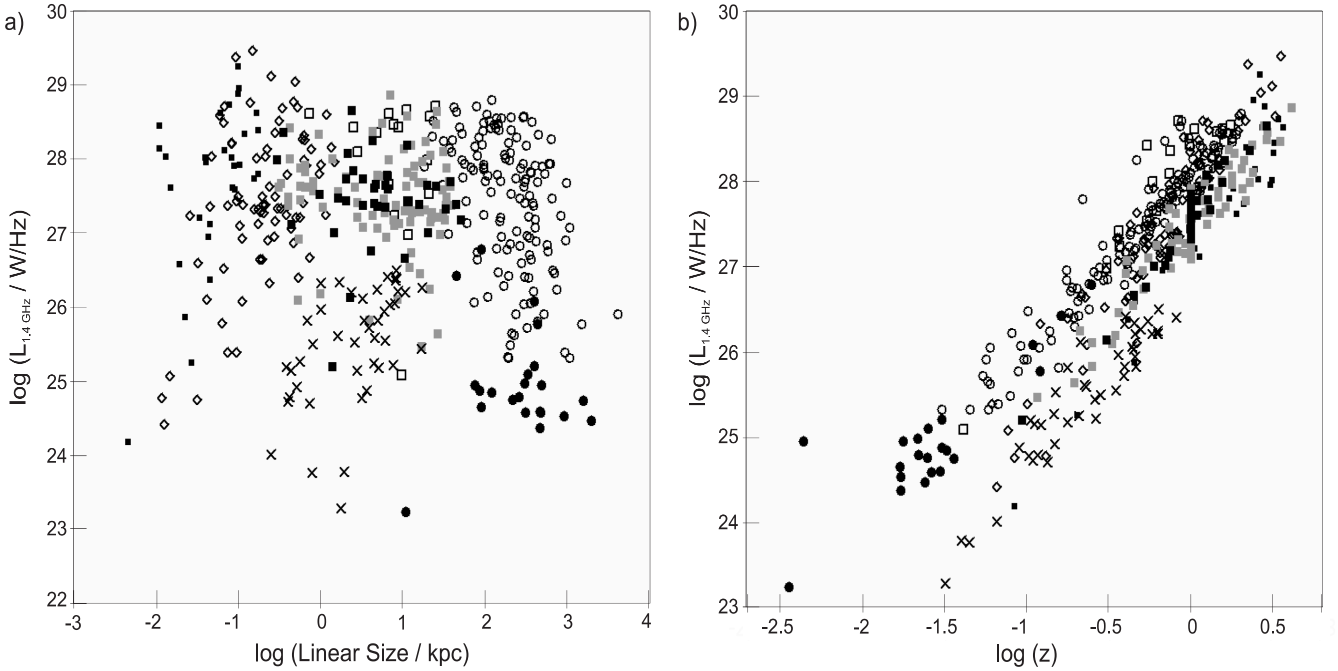

Figure 4. a) Luminosity-size diagram for AGNs, b) Luminosity-redshift diagram for AGNs. Squares indicate CSS sources from samples: Fanti et al. (2001) (grey squares), Marecki et al. (2003a) (black squares), Laing at al. (1983) (empty squares). The diamonds indicate GPS objects and small black squares indicate HFP objects from sample Labiano et al. (2007). The filled circles indicate FR I objects and open circles indicate FR IIs from sample Laing at al. (1983). The crosses indicate the current sample of LLC sources except source with the redshift indicated as '?'.

and twisted jets in 0846+017 and 1154+435 (Fig. 1 and Fig. 2).

Among the LLC sources classified as 'others' we have identified so called 'single-lobed' objects: 0923+079, 1156+470 and 1550+444, based on their radio morphology and position of the optical counterpart (Fig. 3). In the case of two sources (0923+079, 1156+470) about 60 % of the total flux density is missing in our MERLIN observations, which may suggest that they indeed possess another component, but too weak and extended to be detected in a snapshot mode with MERLIN. The 5 GHz MERLIN observations made for all three sources revealed, in two cases (0923+079, 1156+470), very weak central emission which is probably radio core, and breaking up, fading radio lobe in all cases. This kind of objects have been already observed in one of the previous samples of CSS sources (Marecki et al. 2003a), and amongst large-scale sources (Subrahmanyan et al. 2003).

The last three objects belong to the category 'others' we labelled as the 'interacting systems', and these are: the two galaxy pairs (0854+210, 1506+345), and a very compact quasar binary (1641+320) which will be discussed in detail in a separate paper (Fig. 2). It has to be noted here that interpretation of 0854+210 as a galaxy pair has not been confirmed yet by detailed optical study. Two of these sources - 0854+210 and 1506+345 - belong to group of radio-excess *IRAS* galaxies (Drake et al. 2003). The radio powers of compact radio-excess galaxies are generally lower than the well known CSS objects, with a median of $\sim 10^{24.5}$ W Hz^{-1} at 5 GHz, and the lower jet energy fluxes are responsible for that (Drake et al. 2003). Also their morphologies do not resemble typical CSS/GPS sources with symmetric double lobes. They rather appear to be highly disrupted which is consistent in all three objects observed by us. 0854+210 has an extended weak emission indicating a trace of previous activity, and 1506+345 has a complex 5 GHz morphology which is probably a consequence of galaxy-galaxy interactions. The galaxy pair 1506+345 has been also observed in a CO line survey made by Mazzarella et al. (1993), which revealed that both components of this interacting pair contain $\sim 10^{10}\ M_{\odot}$ of molecular gas each. According to the authors what we observe here is a colliding disc galaxies which will evolve into gas-rich galaxy. A young phase of radio activity has been ignited here.

Summing up we have observed four main categories of radio morphology (Table 2) among LLC sources and the most interesting cases among them have been described above. It is difficult to compare radio morphologies of LLC sources with those observed in previous samples (Fanti et al. 2001; Marecki et al. 2003a) because of different observing frequencies and resolutions. However, what we can confirm is that the fraction of sources with complex morphologies (breaking up structures and with single lobe) is higher than that reported in Fanti et al. (2001) and Marecki et al. (2003a). We suggest in section 4.2 that many of them can be interpreted as short-lived objects.

4.2 Evolution of CSS sources

Fig. 4a shows a full range of luminosity and size covered by radio sources and can be used to study the radio source evolution. We propose an evolutionary scheme that is based on these observed parameters in Fig. 5. The flattening of the slope at small size visible on the diagram is real and has been first reported by O'Dea & Baum (1997) suggesting different

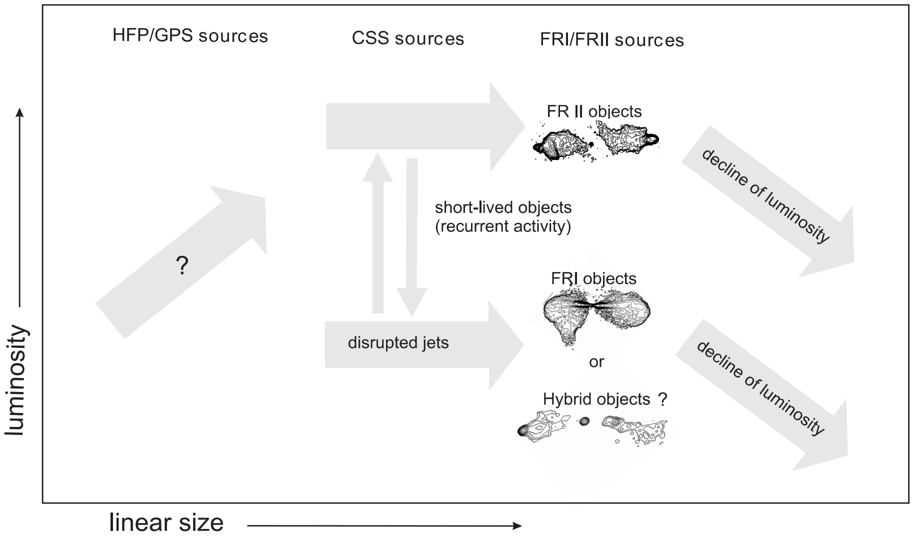

Figure 5. Evolutionary scheme of radio-loud AGNs.

evolution and excess of compact objects comparing to the large scale radio sources. Snellen et al. (2000) discussed the evolutionary scheme of radio sources and concluded that the radio luminosities of GPS sources increase as they evolve, reach a maximum in the CSS phase and then gradually decrease as these objects grow further to become FR II/FR I sources. However, to match observations, the radio jets of the young sources must slow down as they cross the host ISM and dim faster than predicted. Recently de Vries et al. (2009) showed that indeed the expansion speed of GPS radio sources is correlated with their radio luminosity and is lower for less powerful young radio sources. Most of the GPS and CSS sources known so far are powerful objects and the clue to solve the evolution puzzle can be in the analysis of less powerful compact sources.

According to the latest theoretical predictions (Kaiser & Best 2007; Czerny et al. 2009) and observational facts (Gugliucci et al. 2005; Kunert-Bajraszewska et al. 2006) the situation in the group of young radio objects can be complicated. The episodic nature of the radio activity is a fact among large scale objects where we observe two or more of active periods in the radio images. This is still debated for young objects, as is the nature of the mechanism causing it. Based on our latest observations of LLC sample we suggest we should treat the 'young source phase' of the evolution of radio object as the one which determines its further evolution. Different mechanisms and interactions may play an important role here. The most likely mechanism to produce these effects is interaction of the radio source with the host environment. Labiano et al. (2009) found that the GPS and CSS sources (galaxies and quasars) show a strong correlation between [O III]λ5007 line luminosity and size of the radio source suggesting a possible deceleration in the jet as it crosses the host ISM. However this correlation may not be present in fainter radio sources where the radio and [O III]λ5007 can be produced in a different way (Paper II). There are indications (Tasse et al. 2008), based on the environmental studies of radio sources at moderate redshifts (z$\sim$ 0.5-1), that low-luminosity radio AGNs lie in denser environments than the powerful objects, have lower stellar masses and show excess mid-IR emission consistent with a hidden radiatively efficient active nucleus. Tasse et al. (2008) also argue that the low luminosity radio activity is associated with the re-fuelling of massive black holes. Recently Czerny et al. (2009) discussed mechanism of instabilities in the accretion flow suggesting that the duration of the active phase should be longer than 10^4 years to enable the young source to escape from the host galaxy. For the shorter active phase the radio source will be confined within the host galaxy and such short outbursts may occur many times. We have presented this scenario on the scheme of the radio source evolution as the two-sided arrows (Fig. 5) and labeled these sources as short-lived objects. To this group of objects belong observed by us CSSs with weak breaking up structures, without compact hotspots or jets and core visible, which means compact but already fading objects that will not evolve into large scale sources in this phase of activity. We interpret some double sources (0821+321, 1558+536) and 'single-lobed' objects (0923+079, 1156+470, 1550+444) observed in LLC sample as compact faders. We suggest that these double objects from our sample with brightness and polarization asymmetry may undergo disturbed evolution and starting to fade away as single-lobed objects or to become FR Is or hybrids. According to Alexander (2000) sources with disrupted jets are not expected to evolve into FR I objects, but fade so strongly that they become virtually undetectable. Also sources we called 'interacting systems' (galaxy pairs and quasar binaries) can be interpreted as short-lived objects. The galaxy-ISM interactions observed in these double systems can change the direction of the jets and disturb the environment fuelling the black hole and consequently prevent the growing of the radio structure. As an effect of such interactions we observe complicated radio structures consisting of weak fading emission together with current phase and direction of the activity. Two of the weak 'interacting systems' (0854+210 and 1506+345) are radio-excess *IRAS* galaxies. As has been discussed by Drake et al. (2003) the radio-excess sources, with the radio powers in general lower than the well known CSS objects, are not expected to evolve in the same manner as CSS/GPS sources, but rather fade even further to return to their place among the radio-quiet FIR-luminous AGNs.

The evolutionary path for powerful compact objects is the one established so far namely that the CSS sources evolve to become FR IIs.

According to Snellen et al. (2000) and also visible in our plot (Fig. 4a), the smallest radio objects (GPS/HFP sources) should increase their luminosity and size during the evolution. However in the evolutionary scheme (Fig. 5) we put a question mark while illustrating this path. We have noticed that most of the GPS/HFP sources are already as bright as CSSs and FR IIs, and these small objects with lower luminosity can either follow the predicted path or fade earlier becoming weak CSS object.

Another question mark in the evolutionary scheme (Fig. 5) concerns the rare class of radio sources - hybrids, which evolutionary path is suggested by Kaiser & Best (2007). However, recent results based on Chandra observations show that hybrid sources which show broad-line optical spectra have X-ray properties comparable with those of FR IIs radio galaxies (Miller et al. 2009). It is possible that in the case of these rare objects the transition from FR II-type jet to FR I-type plum structure takes place at the later stages of evolution due to interaction with a dense and non-homogeneous intergalactic medium. Numerical works (e.g. Meliani et al. 2008) suggest that a powerful FR II-type jet can be decelerated by a high density medium and transform to FR I-type.

5 SUMMARY

In this paper, we have presented results from MERLIN L-band and C-band observations of a new sample of low luminosity compact sources. Most of the sources have been resolved showing complex, asymmetric radio morphologies suggesting presence of dense environment and jet-ISM interactions. We suggest that some of the sources with the breaking up structures or one-sided morphology are candidates for compact faders. In this case the fraction of faders is higher (∼15%) than that reported in CSS samples from B3-VLA and FIRST catalogues (∼4%). We suspect we can increase the number of these sources by a factor of 2 or even 3, by extending the studies to lower frequencies and luminosities.

We studied correlation between radio power and linear size, and redshift with a larger sample that included also published samples of compact objects and large scale FR IIs and FR Is. The low luminosity compact objects occupy the space in radio power versus linear size diagram below the main evolutionary path of radio objects. We conclude that many of them can be short-lived objects, at least in the current phase of evolution. These undergo disrupted evolution many times as they are be able to escape the host galaxy and evolve to FR IIs. The presented here analysis of the radio properties of LLC sources and also analysis of their spectroscopic features which will be discussed in a second paper of the series indicate that most of them will evolve finally to FR II. However, we suggest that there exists a much larger population of short-lived low luminosity compact objects unexplored so far and among them we can find precursors of large scale FR Is.

ACKNOWLEDGMENTS

We thank Peter Thomasson and Anita Richards for their help with MERLIN observations and data reduction. MERLIN is a UK National Facility operated by the University of Manchester on behalf of STFC.

The research has made use of the NASA/IPAC Extragalactic Database (NED) which is operated by the Jet Propulsion Laboratory, California Institute of Technology, under contract with the National Aeronautics and Space Administration.

This research has made use of Sloan Digital Sky Survey. Funding for the SDSS and SDSS-II has been provided by the Alfred P. Sloan Foundation, the Participating Institutions, the National Science Foundation, the U.S. Department of Energy, the National Aeronautics and Space Administration, the Japanese Monbukagakusho, the Max Planck Society, and the Higher Education Funding Council for England. The SDSS Web Site is http://www.sdss.org/. The SDSS is managed by the Astrophysical Research Consortium for the Participating Institutions. The Participating Institutions are the American Museum of Natural History, Astrophysical Institute Potsdam, University of Basel, University of Cambridge, Case Western Reserve University, University of Chicago, Drexel University, Fermilab, the Institute for Advanced Study, the Japan Participation Group, Johns Hopkins University, the Joint Institute for Nuclear Astrophysics, the Kavli Institute for Particle Astrophysics and Cosmology, the Korean Scientist Group, the Chinese Academy of Sciences (LAMOST), Los Alamos National Laboratory, the Max-Planck-Institute for Astronomy (MPIA), the Max-Planck-Institute for Astrophysics (MPA), New Mexico State University, Ohio State University, University of Pittsburgh, University of Portsmouth, Princeton University, the United States Naval Observatory, and the University of Washington.

REFERENCES

Alexander, P.: 2000, MNRAS 319, 8

Czerny, B., Siemiginowska, A., Janiuk, A., Nikiel-Wroczyński, B., Stawarz, Ł., 2009, ApJ, 698, 840

Drake, C. L., McGregor, P.J., Dopita, M.A., van Breugel, W.J.M., 2003, AJ, 126, 2237

Fanaroff, B. L., & Riley, J. M.: 1974, MNRAS 167, 31

Fanti, C., Pozzi, F., & Dallacasa, D., et al.: 2001, A&A 369, 380

Gawroński, M. P., Marecki, A., Kunert-Bajraszewska, M. & Kus, A. J.: 2006, A&A 447, 63

Giroletti, M., Giovannini, G., & Taylor, G. B.: 2005, A&A 441, 89

Gopal-Krishna, & Wiita, P. J.: 2000, A&A 363, 507

Gugliucci, N. E., Taylor, G. B., Peck, A. B., & Giroletti, M.: 2005, ApJ 622, 136

Holt, J., Tadhunter, C. N., & Morganti, R., 2006, AN, 327, 147

Kaiser, C. R., & Best, P. N.: 2007, MNRAS 381, 1548

Kunert-Bajraszewska, M., & Labiano, A., 2010, MNRAS, in press (Paper II)

Kunert-Bajraszewska, M. & Thomasson, P.: 2009, AN, 330, 210

Kunert-Bajraszewska, M., Marecki, A., & Thomasson, P.: 2006, A&A 450, 945

Kunert-Bajraszewska, M., Marecki, A., Thomasson, P., & Spencer, R. E.: 2005, A&A 440, 93

Labiano, A., 2009, AN, 330, 241

Labiano, A., Barthel, P.D., O'Dea, C.P., et al., 2007, A&A, 463, 97

Labiano, A., O'Dea, C.P., Gelderman, R., et al., 2005, A&A, 436, 493

Laing, R. A., Riley, J. M., & Longair, M. S.: 1983, MNRAS 204, 151

Marecki, A., Spencer, R. E., & Kunert, M., 2003b, PASA 20, 46

Marecki, A., Niezgoda, J., Włodarczak, J., Kunert, M., Spencer, R. E., & Kus, A. J.,2003a, PASA 20, 42

Marecki, A., Kunert-Bajraszewska, M., & Spencer, R. E.: 2006, A&A 449, 985

Mazzarella, J. M., Graham, J. R., Sanders, D. B., Djorgovski, S., 1993, ApJ, 409, 170

Meliani Z., Keppens R., Giacomazzo B., 2008, A&A, 491, 321

Miller B. P., Brandt W. N., 2009, ApJ, 695, 755

O'Dea, C. P., & Baum, S. A., 1997, AJ 113, 148

Saikia, D. J., Jeyakumar, S., Salter, C. J., et al.: 2001, MNRAS 321, 37

Snellen, I. A. G., Schilizzi, R. T., Miley, G. K., de Bruyn, A. G., Bremer, M. N., Röttgering, H. J. A., 2000, MNRAS, 319, 445

Snellen, I. A. G., Schilizzi, R. T., Miley, G. K., Bremer, M. N., Röttgering, H. J. A., van Langevelde, H. J., 1999, NewAR, 43, 675

Subrahmanyan, R., Beasley, A. J., Goss, W. M., Golap, K., & Hunstead, R. W.: 2003, AJ 125, 1095

Tasse, C., Best, P. N., Röttgering, H., Le Borgne, D., 2008, A&A, 490, 893

de Vries, N., Snellen, I. A. G., Schilizzi, R. T., Mack, K.-H., Kaiser, C. R., 2009, A&A, 498, 641

Xiang, L., Dallacasa, D., Cassaro, P., Jiang, D., Reynolds, C., 2005, A&A, 434, 123

APPENDIX A: COMBINED SAMPLE OF CSS SOURCES

Table A1 consists of a large sample of CSS sources which includes last published CSS samples by Fanti et al. (2001) and Marecki et al. (2003a). The data were updated by using the most actual version of the SDSS/DR7 and were used for evolution study presented in Fig.4 and Paper II.

Table A1. Combined sample of CSS sources

Source Name (1)	RA h m s (2)	Dec ° ′ ″ (3)	z (4)	$S_{1.4}$ Jy (5)	$\log L_{1.4}$ W Hz^{-1} (6)	$S_{4.85}$ Jy (7)	$\log L_{4.85}$ W Hz^{-1} (8)	LAS ″ (9)	LLS h^{-1} kpc (10)
2358+406	00 00 53.1	40 54 02	1.000	1.300	27.84	0.688	27.56	0.08	0.64
0003+387	00 06 20.6	39 00 28	1.470	0.482	27.82	0.112	27.19	1.30	11.09
0034+444	00 36 53.5	44 43 21	2.790	0.675	28.65	0.173	28.06	3.20	25.54
0039+391	00 41 54.9	39 25 21	1.006	0.315	27.23	0.069	26.57	0.34	2.74
0039+373	00 42 07.1	37 39 36	1.006	0.939	27.70	0.228	27.09	0.10	0.81
0039+398	00 42 17.4	40 09 48	1.000	0.748	27.60	0.200	27.02	3.70	29.79
0039+412	00 42 18.5	41 29 26	1.000	0.371	27.29	0.129	26.83	2.00	16.10
0041+425	00 44 39.2	42 48 02	1.000	0.463	27.39	0.146	26.89	1.00	8.05
0049+379	00 52 16.8	38 15 28	1.700*	0.793	28.20	0.192	27.58	1.45	12.40
0110+401	01 13 17.8	40 26 13	1.479	0.546	27.88	0.283	27.60	3.90	33.28
0120+405	01 23 26.2	40 46 59	0.840	0.608	27.32	0.199	26.83	2.40	18.38
0123+402	01 25 59.2	40 28 37	1.000	0.256	27.13	0.066	26.54	1.10	8.86
0128+394	01 31 29.5	39 42 58	0.929	0.327	27.16	0.062	26.43	2.70	21.32
0137+401	01 40 33.7	40 24 14	1.620	0.287	27.70	0.113	27.30	4.20	35.94
0140+387	01 43 33.0	39 02 11	2.900*	0.426	28.50	0.063	27.67	0.70	5.53
0144+432	01 47 55.6	43 32 15	1.260	0.334	27.50	0.085	26.90	4.00	33.64
0147+400	01 50 19.6	40 17 30	1.000	0.716	27.58	0.259	27.14	0.10	0.80
0213+412	02 16 30.3	41 31 51	0.515	0.541	26.75	0.259	26.43	2.00	12.39
0222+422	02 25 32.0	42 29 41	3.500*	0.260	28.48	0.066	27.88	3.40	25.33
0228+409	02 31 38.8	41 09 54	1.000	0.351	27.27	0.115	26.78	3.80	30.59
0254+406	02 57 50.2	40 50 32	1.224	0.497	27.64	0.154	27.13	4.50	37.69
0255+460	02 58 30.2	46 16 06	1.210	0.713	27.78	0.256	27.34	0.66	5.52
0701+392	07 04 31.3	39 11 23	1.283	0.503	27.69	0.170	27.22	1.80	15.17
0703+468	07 06 48.0	46 47 56	1.000	1.585	27.92	0.625	27.52	0.08	0.64
0722+393	07 25 50.0	39 17 25	1.000	1.104	27.76	0.236	27.09	0.25	2.01
0729+437	07 32 43.7	43 35 41	1.000	0.385	27.31	0.132	26.84	1.30	10.47
0744+464	07 47 43.6	46 18 58	2.926	0.514	28.59	0.134	28.00	1.40	11.03
0748+413	07 52 19.9	41 15 53	1.000	0.234	27.09	0.067	26.55	0.40	3.22
0754+396	07 58 08.8	39 29 28	2.119	0.523	28.25	0.134	27.66	2.20	18.52
0800+472	08 04 13.9	47 04 43	0.510	0.888	26.95	0.333	26.52	1.00	6.16
0805+406	08 09 03.1	40 32 57	1.775*	0.530	28.07	0.183	27.60	2.50	21.36
0809+404	08 12 53.1	40 19 00	0.551	1.062	27.11	0.446	26.73	1.20	7.70
0810+460	08 14 30.3	45 56 40	0.620	1.106	27.25	0.276	26.65	0.63	4.28
0814+441	08 17 36.0	43 59 35	1.000	0.289	27.18	0.079	26.62	4.00	32.20
0822+394	08 25 23.7	39 19 46	1.210	1.198	28.01	0.341	27.46	0.05	0.42
0840+424	08 43 31.6	42 15 30	1.000	1.409	27.87	0.583	27.49	0.08	0.64
0856+406	08 59 59.6	40 24 35	2.290	0.240	28.00	0.042	27.24	0.80	6.66
0902+416	09 05 22.2	41 28 40	1.000	0.496	27.42	0.159	26.92	0.34	2.74
0930+389	09 33 06.9	38 41 50	2.395	0.284	28.12	0.088	27.61	3.70	30.55
0935+428	09 38 16.5	42 38 35	1.291	0.439	27.64	0.136	27.13	1.30	10.97
0951+422	09 54 12.6	42 01 09	1.783	0.428	27.98	0.167	27.57	2.00	17.08
0955+390	09 58 44.3	38 48 22	1.000	0.460	27.38	0.135	26.85	4.80	38.64
1007+422	10 10 24.8	41 59 33	1.000	0.430	27.35	0.141	26.87	0.13	1.05
1008+423	10 11 54.2	42 04 33	1.000	0.593	27.50	0.199	27.02	0.05	0.40
1014+392	10 17 14.2	39 01 23	0.210	1.392	26.25	0.485	25.79	6.10	20.77
1016+443	10 19 48.2	44 08 25	0.330*	0.354	26.10	0.071	25.40	0.11	0.52
1025+389	10 28 44.3	38 44 37	0.361	0.658	26.46	0.336	26.17	3.20	16.07
1027+392	10 30 16.5	38 57 54	1.000	0.385	27.31	0.128	26.83	1.60	12.88
1039+424	10 42 06.3	42 10 31	1.000	0.277	27.16	0.061	26.51	1.50	12.07
1044+454	10 47 33.7	45 08 52	4.100*	0.440	28.87	0.088	28.17	1.00	7.01
1049+384	10 52 11.8	38 11 44	1.018	0.682	27.58	0.202	27.05	0.10	0.81
1055+404	10 58 00.4	40 10 19	1.000	0.369	27.29	0.107	26.75	2.80	22.54
1128+455	11 31 38.9	45 14 51	0.404	2.049	27.07	0.656	26.58	0.90	4.85
1133+432	11 35 56.0	42 58 45	1.000	1.449	27.88	0.442	27.37	0.07	0.56
1136+420	11 38 59.1	41 48 39	0.829	0.459	27.18	0.187	26.79	1.00	7.62
1136+383	11 39 34.0	38 03 42	1.000	0.460	27.38	0.195	27.01	0.05	0.40
1141+466	11 43 39.6	46 21 20	0.116	0.863	25.47	0.132	24.65	8.10	16.86
1143+456	11 46 15.2	45 20 38	0.762	0.711	27.28	0.149	26.60	0.80	5.92
1157+460	12 00 31.2	45 48 42	0.743	1.156	27.46	0.311	26.89	0.80	5.86
1159+395	12 01 49.9	39 19 11	2.370	0.606	28.43	0.261	28.07	0.05	0.41

Table A1. Combined sample of CSS sources

Source Name (1)	RA h m s (2)	Dec ° ′ ″ (3)	z (4)	$S_{1.4}$ Jy (5)	$\log L_{1.4}$ W Hz^{-1} (6)	$S_{4.85}$ Jy (7)	$\log L_{4.85}$ W Hz^{-1} (8)	LAS ″ (9)	LLS h^{-1} kpc (10)
1201+394	12 04 06.8	39 12 18	0.445	0.483	26.54	0.168	26.08	2.10	12.00
1204+401	12 07 06.2	39 54 39	2.066	0.259	27.92	0.058	27.27	1.60	13.51
1212+380	12 14 56.7	37 48 51	1.500*	0.293	27.63	0.067	26.99	0.30	2.56
1216+402	12 18 37.0	40 00 45	0.756	0.366	26.98	0.101	26.42	3.80	28.04
1217+427	12 19 53.8	42 29 51	1.000	0.303	27.20	0.092	26.69	2.70	21.74
1220+408	12 22 35.2	40 36 21	1.000	0.463	27.39	0.121	26.80	4.10	33.01
1225+442	12 27 42.0	44 00 42	0.348	0.384	26.19	0.114	25.66	0.20	0.98
1233+418	12 35 35.7	41 37 07	0.250*	0.690	26.11	0.285	25.73	2.20	8.55
1241+411	12 44 20.0	40 51 37	0.249	0.361	25.83	0.171	25.50	1.00	3.88
1242+410	12 44 49.2	40 48 06	0.813	1.342	27.63	0.707	27.35	0.04	0.30
1313+453	13 16 11.9	45 04 29	1.544	0.667	28.02	0.307	27.68	0.16	1.37
1340+439	13 43 05.9	43 43 24	1.000	0.547	27.46	0.133	26.85	0.07	0.56
1343+386	13 45 36.9	38 23 13	1.853	0.895	28.34	0.399	27.99	0.11	0.94
1350+432	13 52 28.5	42 59 22	2.149	0.170	27.78	0.029	27.01	1.60	13.44
1432+428	14 34 27.8	42 36 20	1.000	0.912	27.68	0.312	27.22	0.04	0.32
1441+409	14 42 59.3	40 44 29	1.000	0.963	27.71	0.331	27.24	0.10	0.80
1445+410	14 47 12.7	40 47 45	0.195	0.409	25.64	0.156	25.22	8.10	26.02
1449+421	14 51 07.3	41 54 41	1.000	0.813	27.63	0.131	26.84	0.08	0.64
1458+433	15 00 30.0	43 09 52	0.927	0.438	27.28	0.121	26.72	1.60	12.63
2301+443	23 03 45.3	44 39 06	1.700*	1.229	28.39	0.274	27.73	0.50	4.28
2302+402	23 04 54.6	40 28 54	1.000	1.163	27.79	0.386	27.31	0.60	4.83
2304+377	23 07 01.0	38 02 42	0.400*	1.487	26.92	0.642	26.56	0.10	0.54
2311+469	23 13 48.1	47 12 15	0.742	1.927	27.69	0.856	27.33	2.40	17.59
2322+403	23 24 48.5	40 40 23	1.000	0.318	27.22	0.089	26.67	3.20	25.76
2330+402	23 32 52.9	40 30 37	1.000	0.831	27.64	0.302	27.20	0.07	0.56
2348+450	23 51 27.8	45 18 30	0.978	0.742	27.57	0.230	27.06	0.20	1.60
2349+410	23 51 52.8	41 21 15	2.046	0.452	28.15	0.106	27.52	1.20	10.14
0744+291	07 48 05.3	29 03 23	1.000	0.480	27.40	0.170	26.95	0.55	4.43
0747+314	07 50 12.3	31 19 48	1.000	1.050	27.74	0.350	27.27	0.25	2.01
0801+303	08 04 42.2	30 12 37	1.452	1.189	28.20	0.404	27.73	1.30	11.08
0811+360	08 14 49.0	35 53 50	1.000	0.580	27.49	0.170	26.95	0.20	1.61
0850+331	08 53 21.1	32 55 01	1.000	0.465	27.39	0.208	27.04	1.95	15.70
0853+291	08 56 01.2	28 58 35	1.085	0.630	27.61	0.190	27.09	0.80	6.56
0922+322	09 25 32.7	31 59 53	1.000	0.530	27.45	0.200	27.02	1.40	11.27
0949+287	09 52 06.1	28 28 32	1.000	1.364	27.86	0.529	27.45	0.31	2.49
1009+408	10 12 51.8	40 39 04	1.000	0.411	27.34	0.194	27.01	4.06	32.69
1045+352	10 48 34.2	34 57 25	1.604	1.051	28.25	0.439	27.88	0.50	4.28
1056+316	10 59 43.2	31 24 21	0.307*	0.459	26.14	0.209	25.80	0.50	2.25
1059+351	11 02 08.7	34 55 11	0.594*	0.702	27.01	0.252	26.56	3.03	20.17
1123+340	11 26 23.7	33 45 27	1.247	1.320	28.08	0.380	27.54	0.25	2.10
1125+327	11 28 02.4	32 30 47	0.750*	0.600	27.19	0.205	26.72	6.81	50.10
1126+293	11 29 21.7	29 05 06	1.000	0.729	25.20	0.213	24.67	0.79	1.37
1132+374	11 35 05.9	37 08 41	2.880	0.638	28.66	0.218	28.20	0.30	2.37
1232+295	12 34 54.4	29 17 44	1.000	0.460	27.38	0.160	26.93	0.40	3.22
1236+327	12 39 09.1	32 30 27	1.000	0.832	27.64	0.256	27.13	3.12	25.12
1242+364	12 44 49.7	36 09 26	1.000	0.780	27.61	0.210	27.04	0.55	4.43
1251+308	12 53 25.7	30 36 35	1.311	0.450	27.67	0.200	27.32	0.55	4.65
1302+356	13 04 34.5	35 23 34	1.000	0.483	27.40	0.185	26.99	0.20	1.61
1315+396	13 17 18.6	39 25 28	1.562	0.615	27.99	0.227	27.56	0.03	0.29
1334+417	13 36 26.4	41 31 13	1.000	0.470	27.39	0.154	26.91	5.47	44.04
1401+353	14 03 19.2	35 08 12	0.450*	0.630	26.67	0.180	26.13	1.80	10.35
1407+369	14 09 09.5	36 42 08	0.996*	0.538	27.45	0.216	27.05	0.25	2.01
1425+287	14 27 40.3	28 33 26	1.000	0.859	27.65	0.198	27.02	0.75	6.03
1502+291	15 04 26.7	28 54 31	2.283†	0.567	28.37	0.261	28.03	0.04	0.35
1542+323	15 44 48.4	32 08 45	1.000	0.854	27.65	0.325	27.23	2.41	19.40
1601+382	16 03 35.1	38 06 43	1.000	0.430	27.35	0.200	27.02	0.75	6.04
1616+366	16 18 23.6	36 32 02	0.734	0.536	27.12	0.268	26.82	0.06	0.44
1619+378	16 21 11.3	37 46 05	1.273	0.640	27.79	0.200	27.28	0.75	6.32
1627+289	16 29 12.3	28 51 34	1.000	0.526	27.44	0.162	26.93	0.65	5.23

Table A1. Combined sample of CSS sources

Source Name (1)	RA h m s (2)	Dec ° ′ ″ (3)	z (4)	$S_{1.4}$ Jy (5)	$\log L_{1.4}$ W Hz^{-1} (6)	$S_{4.85}$ Jy (7)	$\log L_{4.85}$ W Hz^{-1} (8)	LAS ″ (9)	LLS h^{-1} kpc (10)
1632+391	16 34 02.9	39 00 00	1.085	0.930	27.78	0.370	27.38	0.80	6.56
1656+391	16 58 22.2	39 06 26	1.000	0.650	27.53	0.240	27.10	0.12	0.97
1709+303	17 11 19.9	30 19 18	1.000	1.030	27.73	0.370	27.29	0.40	3.22
1717+315	17 19 30.0	31 28 48	1.000	0.450	27.38	0.150	26.89	0.60	4.83
1723+406	17 25 16.3	40 36 41	1.000	0.962	27.71	0.221	27.07	4.65	37.44

Description of the columns: (1) source name; (2) and (3) source coordinates (J2000); (4) redshift; $*$ - photometric redshift taken form the literature or from the SDSS; † - this is a new value from the SDSS; we adopt $z = 1.0$ for sources with unknown redshift; (5) total flux density at 1.4 GHz extracted from FIRST; (6) log of the radio luminosity at 1.4 GHz; (7) total flux density at 4.85 GHz extracted from GB6; (8) log of the radio luminosity at 4.85 GHz; (9) largest angular size (LAS); (10) largest linear size (LLS) calculated based on the largest angular size measurements on resolved structure taken from the literature. Data are taken from Fanti et al. (2001) sample (first part of the table) and Marecki et al. (2003a). sample. There is a small overlap of this two samples that is why the overlaping sources are included only in a first part of the table.